Petroleum Science 22 (2025) 4992–5004

Contents lists available at ScienceDirect

Petroleum Science

journal homepage: www.keaipublishing.com/en/journals/petroleum-science

Original Paper

Focusing mechanism and anisotropy correction of array induction logging responses for shale reservoirs in horizontal wells

Lei Wang [a,b], Kang-Kang Wu [a,b], Ying-Ming Liu [c,*], Xiao-Kai Xu [d], Shao-Gui Deng [a,b], Ping Qiao [a,b]

[a] State Key Laboratory of Deep Oil and Gas, China University of Petroleum (East China), Qingdao, 266580, Shandong, China
[b] School of Geosciences, China University of Petroleum (East China), Qingdao, 266580, Shandong, China
[c] Research Institute of Petroleum Exploration & Development, PetroChina, Beijing, 100083, China
[d] Sinopec Matrix Corporation, Qingdao, 266001, Shandong, China

A R T I C L E I N F O

Article history:
Received 14 January 2025
Received in revised form
20 May 2025
Accepted 5 August 2025
Available online 11 August 2025

Edited by Meng-Jiao Zhou

Keywords:
Shale reservoirs
Horizontal wells
Array induction logging
Software focusing
Anisotropy correction

A B S T R A C T

We have developed a novel method for correcting resistivity anisotropy in array induction logging (AIL) for shale reservoirs drilled with horizontal wells. This method is featured by two aspects: simplifying software focusing (SF) algorithm from two-dimensional (2D) to one-dimensional (1D) and approximately decoupling the resistivity anisotropy effect. Initially, the typical raw and focused AIL responses are simulated to determine the applicability of the 2D SF algorithm in deviated and horizontal wells. The non-necessity of SF algorithm along vertical direction is also proved for the pure horizontal wells. Subsequently, a 1D SF algorithm that focuses only along the radial direction in horizontal wells is developed to replace the original 2D SF algorithm. This new method eliminates the opacity of traditional SF algorithms and can be easily applied to different AIL tools. The sensitivity of AIL to resistivity anisotropy in homogeneous and layered formations is then discussed, showing that the anisotropy effect can be separated from other effects. Finally, an efficient anisotropy correction scheme using the Levenberg-Marquardt algorithm is established to quickly and accurately correct AIL data in horizontal wells. Results from simulated and measured data demonstrate that this new method effectively removes the anisotropy effect and provides accurate horizontal resistivity for shale beds drilled with horizontal wells. Compared with existing methods, it is significantly faster and compatible with AIL tools from various companies, laying solid foundation for the interpretation and evaluation of shale reservoirs in horizontal wells.

1. Introduction

Shale reservoirs, one of the most important unconventional resources, are well developed in China. These reservoirs are typically characterized by low porosity and permeability, displaying significant resistivity anisotropy and impermeability (Anderson et al., 1995; Hagiwara, 2011; Mallan and Torres-Verdín, 2007; Mohaghegh, 2013; Wang et al., 2023). Unlike conventional oil and gas reservoirs, horizontal well drilling is employed to enhance development efficiency in shale reservoirs (Alpak et al., 2003; Bang et al., 2001; Gorbatenko and Sukhorukova, 2016; Wei et al., 2024). While logging-while-drilling (LWD) electromagnetic measurement is an effective method for in-situ resistivity detection in horizontal wells in real-time, it is often considered too costly (Wang et al., 2022; Zhou et al., 2016a, 2016b). In contrast, domestic companies, constrained by logging expenses, commonly utilize post-drilling logging techniques, such as dual laterolog, dual induction logging, and array induction logging (AIL), to determine reservoir resistivity (Barber et al., 1995; Zhou et al., 1994). Given that shale formations typically employ oil-based mud (OBM) to prevent borehole collapse, AIL has gained popularity (Alpak et al., 2006; Wang, 2011).

AIL can provide plenty resistivity curves with identical vertical resolution and different radial detection depths, making it a frequently employed tool in the evaluation of unconventional

* Corresponding author.
E-mail address: liuym_mail@aliyun.com (Y.-M. Liu).
Peer review under the responsibility of China University of Petroleum (Beijing).

https://doi.org/10.1016/j.petsci.2025.08.009
1995-8226/

reservoirs (Barber and Rosthal, 1991; Beste et al., 2000; Ge et al., 2025). The core of AIL lies in measuring numerous raw responses by multiple subarrays and synthesizing them with the 2D software focusing (SF) algorithm (Beard et al., 1996; Li et al., 2019; Zhao et al., 2025). However, the 2D SF algorithm is specifically designed for axially symmetric formations and performs well in vertical wells (Liu et al., 2020; Tarouilly et al., 2003). When applied to deviated and horizontal wells, the focused responses in horizontal wells often exhibit nonlinear behavior and even show "horns" that surpass the true resistivity of reservoirs. Combined with the effects of anisotropy, these measured AIL responses deviate from the true resistivity, significantly impacting the accuracy of reservoir evaluation (Rabinovich et al., 2006; Zhou et al., 2016a, 2016b). Furthermore, the coefficient filter libraries of SF for AIL tools vary among different companies, and the SF algorithms are not publicly disclosed. This complicates the forward modeling and inversion of AIL focused responses, limiting the applicability of data processing methods and impeding the efficient development of shale oil reservoirs. As a result, the efficient extraction of resistivity in horizontal wells of shale reservoirs has emerged as an urgent concern.

The existing correction methods for AIL data in horizontal wells can be divided into two categories. Firstly, by constructing the filter libraries of inclined boreholes under various dipping angles, inclination correction is carried out on the measured data, and then the corrected data is processed using an inversion designed for vertical boreholes (Bai et al., 2018; Hou and Bittar, 2010). Secondly, one-dimensional (1D) forward modeling and inversion methods are employed to conduct inclination correction on the sub-array responses and then refocus the corrected responses (Gao et al., 2007; Løseth and Ursin, 2007; Kong, 1972; Hong et al., 2021; Hu et al., 2020). The former enables real-time data processing, but the construction of the filter libraries is extremely complicated, and the inversion accuracy is low. The latter yields more accurate inversion but fails to meet the requirements of real-time processing. Moreover, the subarray responses before focusing are not available at the oilfield site in most cases. More importantly, both of the above methods are only applicable to highly angle wells with the dipping angle less than 80°, and the effect of data inversion in horizontal wells is relatively poor. Therefore, there is an urgent need to establish an anisotropy correction method of AIL data for horizontal wells in shale reservoirs that possess high accuracy, rapid speed, and strong applicability.

The remainder of this paper is organized as follows. This paper initially analyzes the focusing mechanism of AIL responses, determines the applicable scope and necessity of the 2D SF algorithm in horizontal wells, and establishes a 1D SF algorithm for radial focused responses. Furthermore, the sensitivity of AIL responses to anisotropy is analyzed, and a novel hierarchical correction for the thickness and anisotropy is proposed, which effectively improves the data processing speed while ensuring accuracy. On this basis, an efficient anisotropy correction method for horizontal wells is developed. Finally, the advantages of the new correction method are validated through comparison with the commercial software LogXD™. Meanwhile, its applicability is verified by applying it to process the data of various AIL tools within the same horizontal well.

2. Focusing mechanism of array induction logging (AIL) responses in horizontal wells

2.1. 2D software focusing algorithm of AIL responses

AIL tools (taking the high definition induction logging (HDIL) as an example) generate alternating electromagnetic fields with 8 frequencies in the formation through the transmitter and measure the induced electromotive force caused by the current in the formation using 7 receivers with different spacing, thus obtaining a total of 56 original responses. Subsequently, a skin effect correction method of multi-frequency is employed to process the original responses (He et al., 2012), and 7 sub-array responses are acquired. Furthermore, seven sub-array responses that are not affected by the borehole are obtained through borehole correction. Finally, the sub-array responses after borehole correction can be processed by 2D SF algorithm to obtain focused signals with fixed vertical resolutions (1, 2 and 4 ft) and different detection depths (10, 20, 30, 60, 90 and 120 inches). The signal with a vertical resolution of 2 ft and a radial detection depth of 90 inches can be named M2R9. The specific process of the above focusing is shown in Fig. 1.

As can be seen from the above process, the SF algorithm consists of the radial resolution focusing and vertical resolution matching techniques. The former constructs the focusing coefficient filter based on a 2D axisymmetric model (vertical well). At this time, the conductivity can be regarded as a 2D function of the vertical and radial directions. After the convolution of the geometric factors and the response of different subarrays, focused signals of multiple radial depths at the same vertical position are obtained. This process can be written as

$$\sigma_{\mathrm{p}}(\rho_k, z) = \sum_{j=1}^{J} \sum_{z'=z_{\min}}^{z_{\max}} w_j^k(z', \sigma)\sigma_{\mathrm{a}}^j(z-z'), \tag{1}$$

where $\sigma_{\mathrm{p}}(\rho_k, z)$ is the conductivity at the radial position ρ_k and the vertical position z after focusing, and the k is the number of detection depths focused, $k = 1, 2, \ldots, 6$. $\sigma_{\mathrm{a}}^j(z)$ is the response of j-th subarray at z, $j = 1, 2, \ldots, 7$. $w_j^k(z', \sigma)$ is the filter of the j-th subarray when the detection depth is ρ_k, and $z = z_{\min} \sim z_{\max}$ is the vertical distance of the focusing. σ is the formation conductivity, which suggests that the focusing filter is a function of the formation conductivity. For a formation with σ, measurements from all subarrays of the range $z = z_{\min} \sim z_{\max}$ can be focused into focused responses at the same vertical depth and at different radial depths by pleating the product of filter $w_j^k(z', \sigma)$ with the σ. The above filter needs to be obtained by using tool parameters, and the filters of different tools are different. After radial resolution focusing, six responses with different detection depths and different vertical resolutions can be obtained. One response with high-resolution is selected as the benchmark, the difference between the adjacent responses is filtered, and then the difference is matched to the corresponding low-resolution response. The above process is called vertical resolution matching.

2.2. Applicability of 2D SF algorithm in horizontal wells

Since the SF algorithm is designed for the vertical well model, it cannot achieve an ideal effect in the horizontal wells, resulting in deviations between the reservoirs evaluation results and the actual formation. Additionally, there are numerous influencing factors in horizontal wells, which makes it extremely difficult to establish a three-dimensional (3D) SF filter coefficient library suitable for the horizontal wells. Therefore, it is particularly important to clarify the applicable scope of the traditional SF algorithm in the horizontal wells. Therefore, based on the SF module of the HDIL tool in the commercial software Express, this section comprehensively analyzed the laws of focused responses under different horizontal wells. This process helps to provide a decision-making basis for the processing and interpretation of the AIL data in horizontal wells on site.

Firstly, in order to clarify the applicability of SF algorithm under different dipping angles, a single-boundary model was

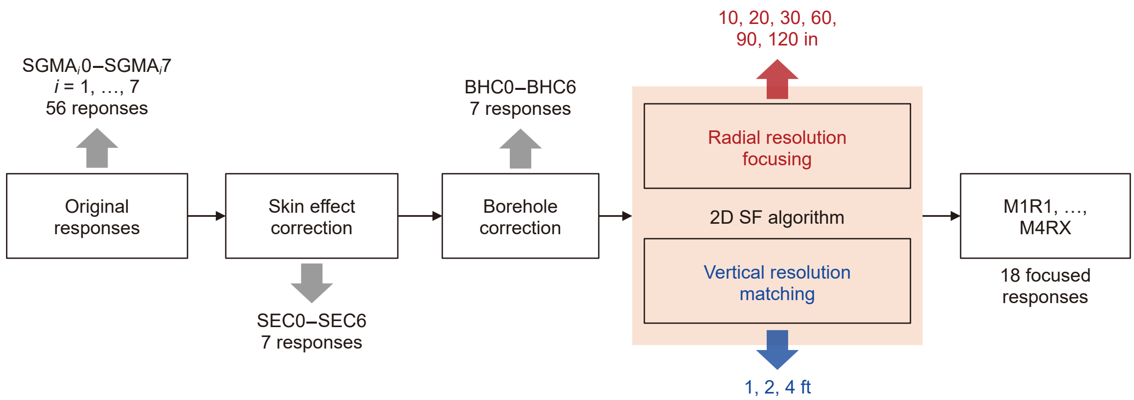

Fig. 1. Focusing process of array induction logging (AIL) responses.

established. The resistivities of the upper and lower layers are 4 Ω·m and 16 Ω·m respectively. Fig. 2(a)–(c) show the responses of the sub-arrays after skin effect correction under different dipping angles α for this model, and Fig. 3(a)–(c) further display the corresponding focused responses. These and the apparent resistivity (R_a) shown in the following figure represent the calculated apparent resistivity of the stratum.

By comparing Figs. 2 and 3, it can be found that the focused responses coincide with each other, and the responses at different detection depths have the same resolution in vertical well, which can accurately represent the resistivity. As the dipping angle increases, the focused responses near the boundary start to separate. However, when the dipping angle less than 45°, the SF algorithm still has a relatively good effect. Nevertheless, in the horizontal well (89°), the focused responses near the boundary show disorder and exceeding the true resistivity, and these abnormalities are particularly obvious in the high-resistivity layer. Additionally, compared with the sub-array responses, the sub-array responses can detect the boundary at a farther distance, contain richer formation information, and have no obvious abnormal phenomena near the boundary. Therefore, it is recommended to retain the sub-array responses during the horizontal wells logging to facilitate further data processing.

Furthermore, in order to clarify the applicability of SF algorithm under different resistivity contrast in horizontal wells. Firstly, Fig. 4(a)–(c) established single-boundary models with different contrasts C respectively, and presented the sub-array responses when $\alpha = 89°$. The upper layer resistivities of these models are 4 Ω·m.

It can be found that as the resistivity contrast increases, the sub-array responses undergo nonlinear changes, and the nonlinear is directly proportional to the spacing. When the resistivity contrast is greater than 4, the long spacing sub-array responses present “horns”, and the range of the “horns” is directly proportional to the contrast. At this time, the long-spacing sub-array responses cannot provide accurate resistivity and is difficult to be used for data processing.

The Fig. 5 presents the focused responses corresponding to Fig. 4. It can be seen that when the resistivity contrast is less than or equal to 2, the focused responses can represent the resistivity relatively accurately, and the abnormal influence of SF algorithm can be ignored in horizontal wells. As the resistivity contrast increases, the nonlinear phenomenon at the boundary becomes more obvious. When the resistivity contrast exceeds 10, the responses of 10, 60 and 90 inches show “horns” that far exceed the true resistivity and cannot be used for data processing. In

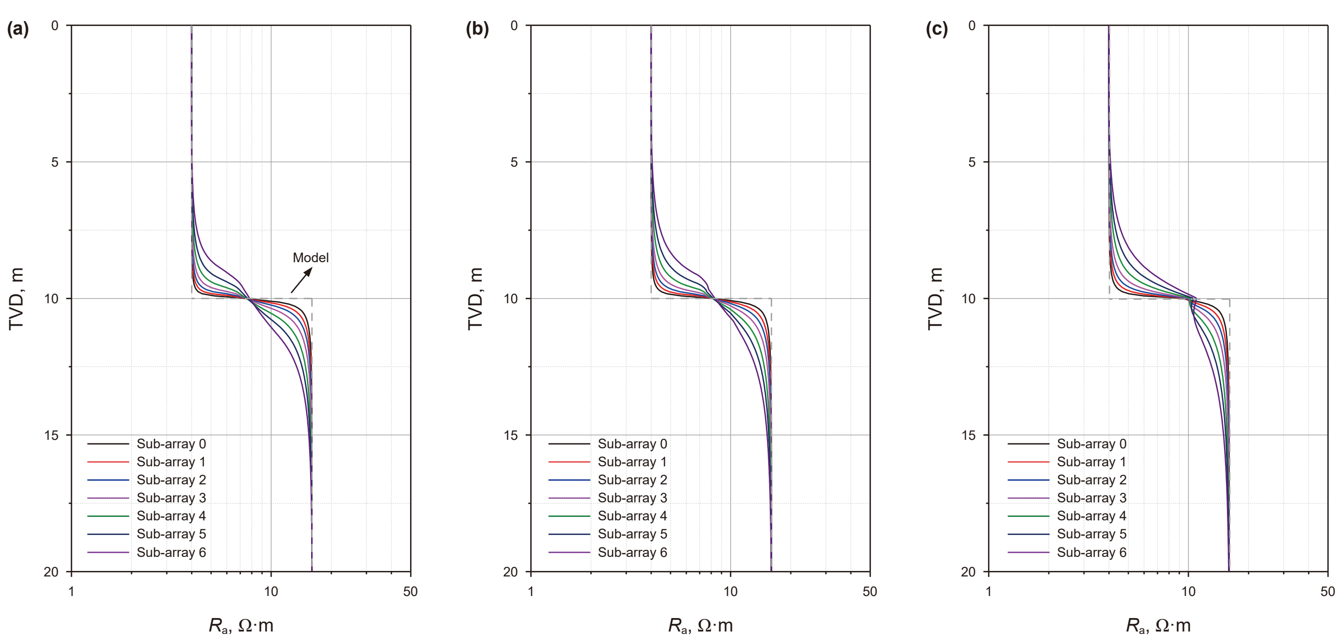

Fig. 2. Sub-array responses in different dipping angles: **(a)** $\alpha = 0°$; **(b)** $\alpha = 45°$; **(c)** $\alpha = 89°$. R_a represents the calculated apparent resistivity of the formation.

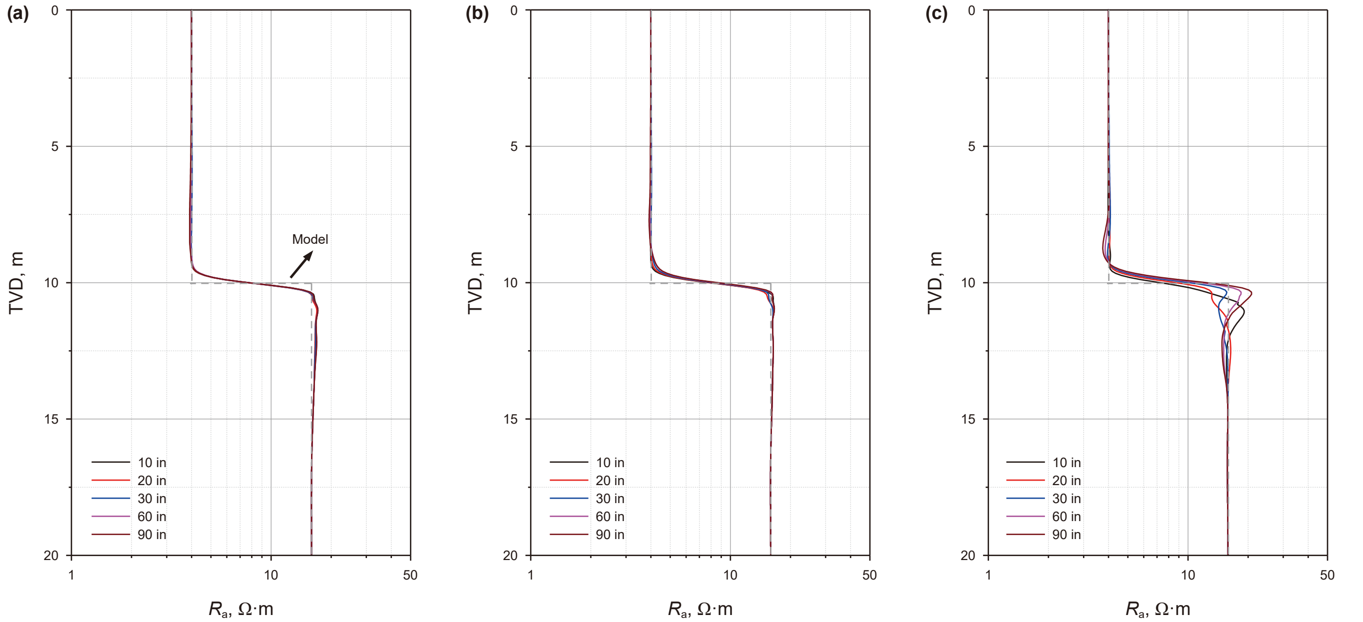

Fig. 3. Focused responses in different dipping angles: **(a)** $\alpha = 0°$; **(b)** $\alpha = 45°$; **(c)** $\alpha = 89°$.

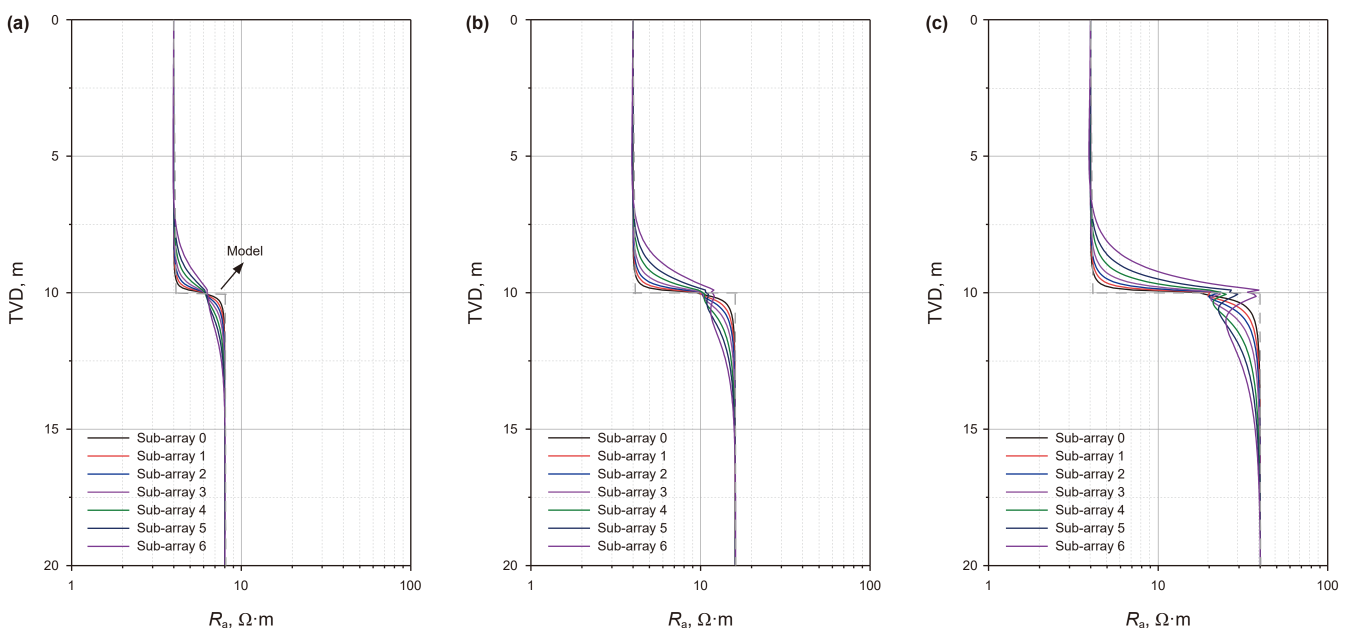

Fig. 4. Sub-array responses in different resistivity contrasts when $\alpha = 89°$: **(a)** $C = 2$; **(b)** $C = 5$; **(c)** $C = 10$. C represents the contrast in resistivity of the formation on both sides of the interface in the single-boundary model.

contrast, the responses of 20 and 30 inches are less affected by SF algorithm. It is recommended to give priority to using these two responses in the data processing.

2.3. Non-necessity of 2D SF algorithm along vertical direction

The principle of vertical focusing of SF algorithm is to obtain the sub-array responses within the apparent depth of 10 m above and below the current logging point, and then use the resolution differences among each sub-array response to compensate each other, so as to achieve the purpose of improving the resolution. Therefore, the effect of vertical focusing mainly depends on the vertical differences among the apparent depth points. That is to say, the greater the vertical differences are, the more obvious effect will be. This is the reason why the SF algorithm performs well in vertical wells. However, as the dipping angle increases, the vertical distance for focusing is shortened, and the vertical differences are reduced. In horizontal wells, there is almost no difference among the vertical responses of different apparent depths, resulting in the failure of vertical focusing. Therefore, the vertical focusing in horizontal wells is not necessary. Fig. 6 further shows the vertical focusing scopes of the AIL signals under different dipping angles.

To further verify the accuracy of the above conclusions, this part analysis the responses before and after SF algorithm under

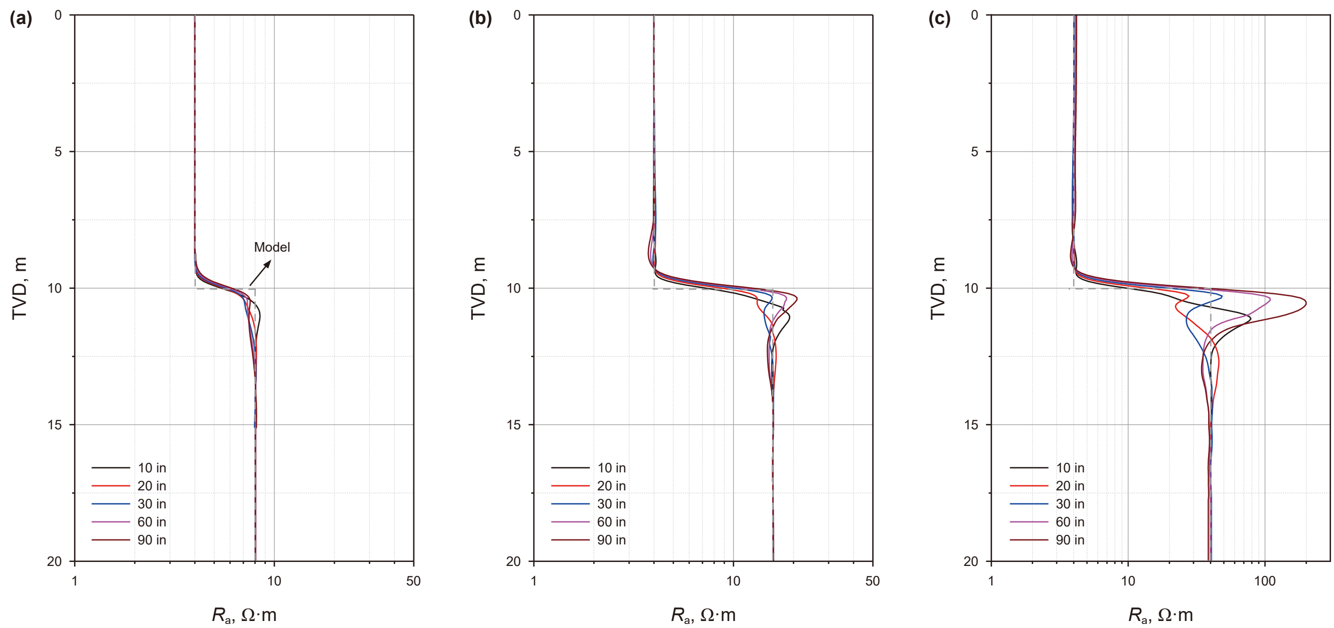

Fig. 5. Focused responses in different resistivity contrasts when $\alpha = 89°$: **(a)** $C = 2$; **(b)** $C = 4$; **(c)** $C = 10$.

different thicknesses. When the AIL tool measures in horizontal wells, the surrounding layers on both sides of the target layer can usually be respectively equivalent by using the geometric factor, and then the formation can be equivalent to a three-layer model. In order to clarify the characteristic of the sub-array responses under different thickness in horizontal wells, Fig. 7(a)–(c) established three-layer models with different thicknesses H of the middle layer, respectively. The resistivities of the surrounding layers of these models are all 5 Ω·m, and the resistivity of the middle layer is 20 Ω·m. Fig. 7(a)–(c) show the sub-array responses of the above models when $\alpha = 89°$.

It can be seen that the sub-array responses are affected by the surrounding layers is directly proportional to the spacing in horizontal wells. The short spacing sub-array responses are less affected by the surrounding layers and can accurately reflect the true resistivity in most cases, but they will still be affected by the thickness in thin layers. On the contrary, the long spacing sub-array responses often deviate from the true resistivity and cannot provide accurate resistivity. Furthermore, in order to compare the effects of SF algorithm in above models, Fig. 8(a)–(c) respectively present the focused responses corresponding Fig. 7. It can be found that the characteristics of the focused responses are consistent with the sub-array responses. Meanwhile, the separation of the focused responses of 10–30 inches is minimal with the thickness greater than or equal to 5 m, and they can relatively accurately represent the true resistivity. Therefore, the responses of 10–30 inches can be used for processing when the thickness exceeds 5 m. By comparing Figs. 7 and 8, it can be seen that the focused responses do not have an improvement in resolution. This preliminarily illustrates the loss of vertical focusing effect in horizontal wells.

2.4. 1D SF algorithm along radial direction

Based on the above conclusion, the vertical influence term in Eq. (1) can be eliminated to establish a 1D SF algorithm that focuses only on the radial direction. The response of the j-th sub-array under the Doll approximation theory in induction logging can be expressed as

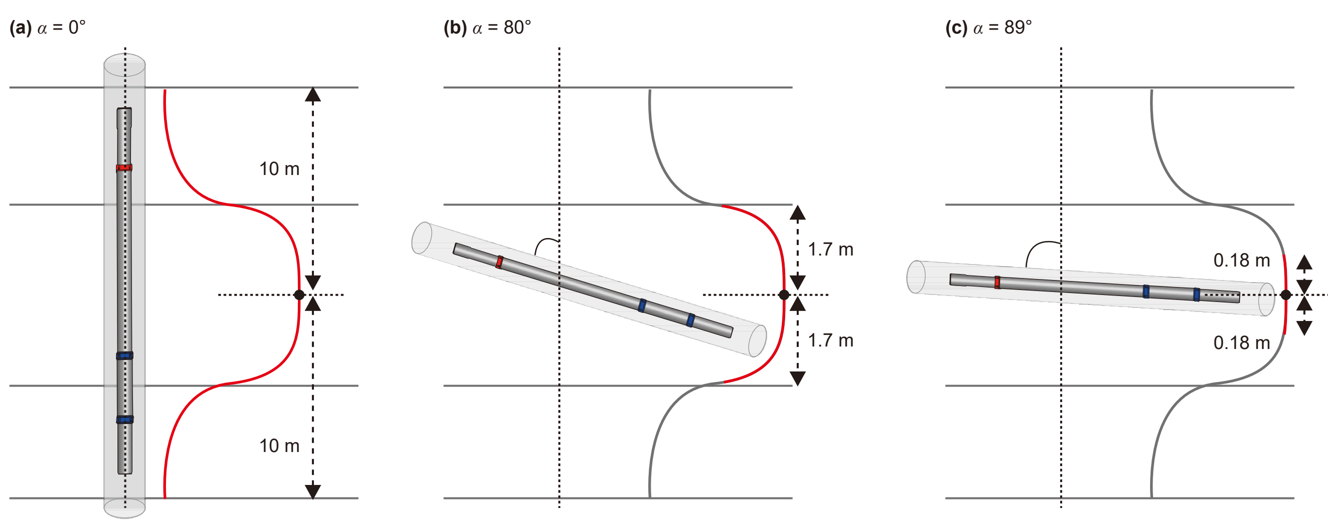

Fig. 6. Vertical focusing scopes under different dipping angles: **(a)** $\alpha = 0°$; **(b)** $\alpha = 80°$; **(c)** $\alpha = 89°$.

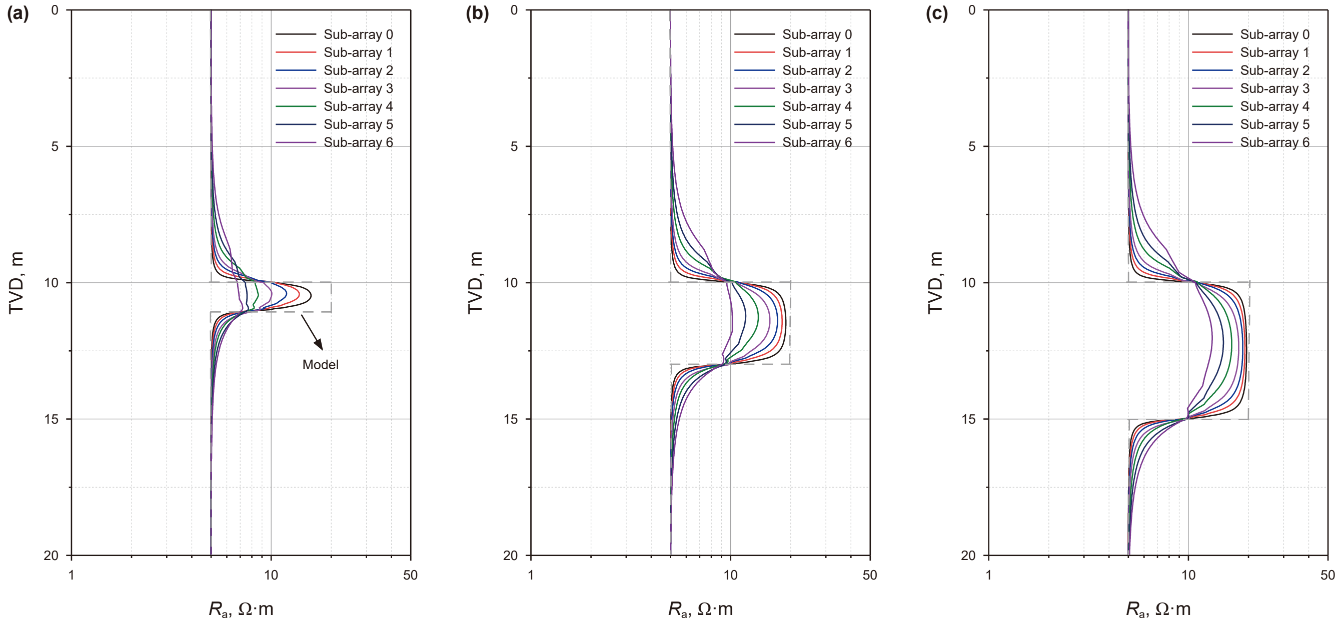

Fig. 7. Sub-array responses in different thicknesses when $\alpha = 89°$: **(a)** $H = 1$ m; **(b)** $H = 2$ m; **(c)** $H = 5$ m.

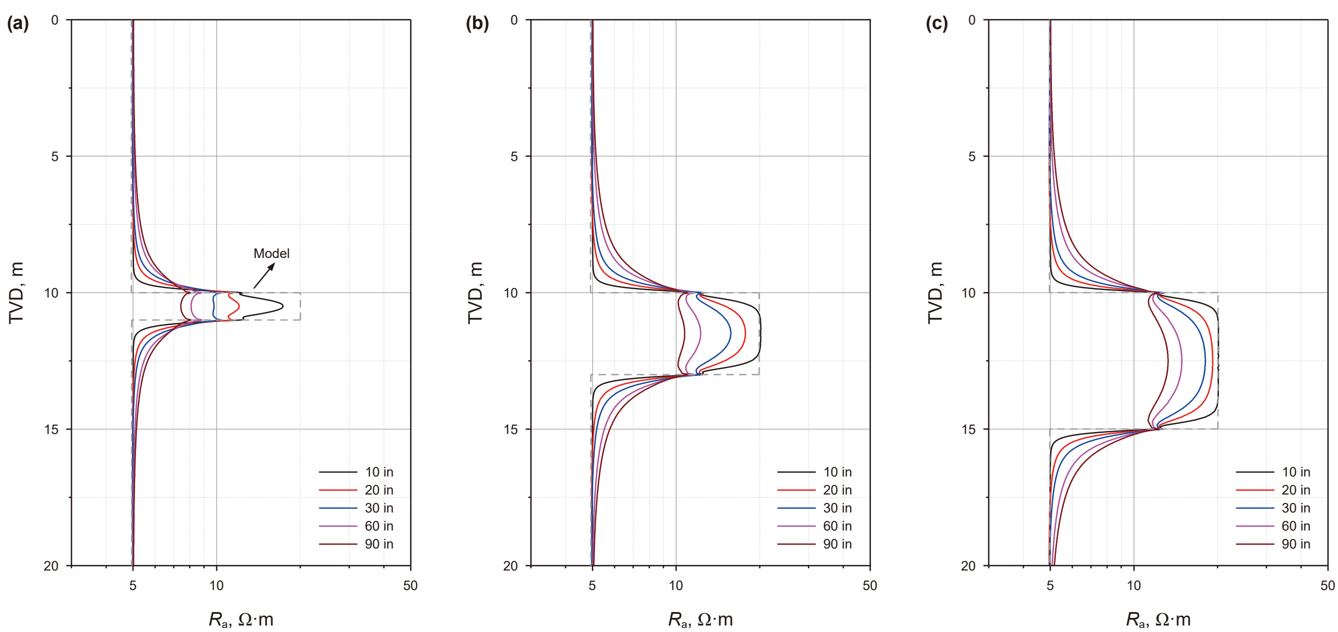

Fig. 8. 2D focused responses in different thicknesses when $\alpha = 89°$: **(a)** $H = 1$ m; **(b)** $H = 2$ m; **(c)** $H = 5$ m.

$$\sigma_a{}^j(z) = \int_{-\infty}^{\infty}\int_{0}^{\infty} g_j(\rho'', z - z'')\sigma(\rho'', z'')\mathrm{d}\rho''\mathrm{d}z'' \tag{2}$$

where $g_j(\rho, z)$ is the 2D Doll differential geometry factor, which is independent of the formation conductivity. Therefore, the focus filter can be written as $w_j^k(z)$. Substitute Eq. (2) into Eq. (1) and exchanging the order of summation and integration yields,

$$\sigma_p(\rho_k, z) = \int_{-\infty}^{\infty}\int_{0}^{\infty}\sum_{j=1}^{7}\sum_{z'=z_{\min}}^{z_{\max}} w_j^k(z')g_j(\rho'', z - z' - z'')\sigma(\rho'', z'')\mathrm{d}\rho''\mathrm{d}z'' \tag{3}$$

Introducing the response functions $g^k(\rho, z)$,

$$\sigma_p(\rho_k, z) = \int_{0}^{\infty}\mathrm{d}\rho''\int_{-\infty}^{\infty} g^k(\rho', z - z')\sigma(\rho'', z'')\mathrm{d}z'' \tag{4}$$

where both z' and z'' represent vertical distances, and both ρ' and ρ'' represent radial distances,

$$g^k(\rho, z) = \sum_{j=1}^{7}\sum_{z'=z_{\min}}^{z_{\max}} w_j^k(z')g_j(\rho, z - z'') \tag{5}$$

Eq. (5) is a 2D focusing function and integrating this equation along the z and ρ directions, respectively, yields a 1D vertical focusing function and a 1D radial focusing function. Among them, the 1D radial focusing function can be written as

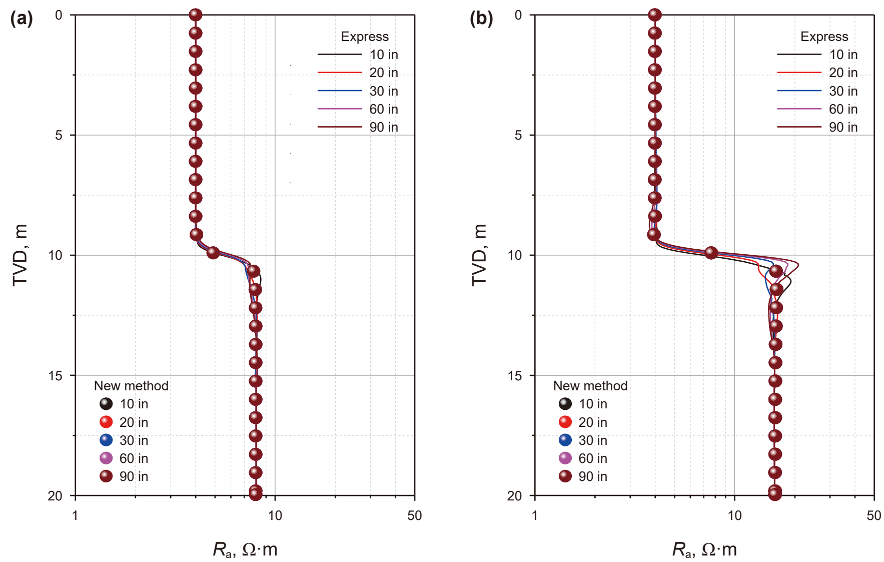

Fig. 9. Comparison of focused responses obtained by Express and our method in different resistivity contrast formations when $\alpha = 89°$: **(a)** $C = 2$; **(b)** $C = 4$.

$$g_{\mathrm{RGF}}^{k}(\rho) = \sum_{\mathrm{j}=1}^{7} W_j^k g_j(\rho), W_j^k = \sum_{z'=z_{\min}}^{z_{\max}} w_j^k(z') \tag{6}$$

Integrating both sides of Eq. (6) along the ρ direction yields

$$G_{\mathrm{RGF}}^{k} = \sum_{j=1}^{7} W_j^k G_j \tag{7}$$

where G_{RGF}^{k} represents the radial integral geometric factor of the focused response for k-th detection depth, and G_j is the radial integral geometric factor of j-th subarray response. w_j^k represents the weight coefficient of the j-th sub-array response corresponding to the focused response of the k-th detection depth. By using polynomial fitting algorithm, the weight coefficients of each sub-array response corresponding to the focused response of each detection depth can be obtained. Eq. (7) can be used to simulate the focused response of k-th detection depth,

$$\sigma_{\mathrm{p}}^{k} = \sum_{j=1}^{7} W_j^k \sigma_{\mathrm{a}}^{j} \tag{8}$$

where σ_{p}^{k} is the response at the k-th detection depth after focusing, and σ_{a}^{j} is the apparent conductivity of the j-th sub-array. This method neglects the vertical influence and enables the rapid simulation of radial focused responses in horizontal wells. Meanwhile, the obtained focused responses can acquire the desired vertical resolution using the Gaussian pulse function. After investigation, it is found that the radial integral geometric factors of the focused responses for AIL tools from various companies are identical, which enhances the applicability of processing method.

In order to verify the effectiveness of the new method for radial focused responses, Fig. 9(a) and (b) compare the focused responses obtained by the new method (dotted lines) and Express (solid lines) for the model in Fig. 5(a) and (b). It can be observed that the focused responses of different detection depths obtained by our method in horizontal wells have the same vertical resolution, and there is almost no disorder or nonlinearity near the boundary, eliminating the abnormal of traditional 2D SF algorithm. Comparing the results of the two methods, the 20 inches and 30 inches responses obtained by Express basically coincide with the results of new method in the low contrast formations. Therefore, the 20 inches and 30 inches responses should be preferentially selected for data processing. Taking the focused results of the 1D SF algorithm as the standard, the relative errors of the 2D SF algorithm under the two models are given in Fig. 10(a) and (b), respectively. It can be found that the error of 2D SF algorithm is proportional to the resistivity contrast in horizontal wells, and the error mainly exists near the boundary. Besides, the error of the 2D SF algorithm is also proportional to the dipping angle, which can be seen from Fig. 3 and will not be repeated here.

To further verify the accuracy of the 1D SF algorithm, Fig. 11 presents a comparison of the responses before and after using SF algorithm in a horizontal well ($\alpha = 89°$). In this figure, the first track (from top to bottom) is the sub-array responses after borehole correction, and the second track is the focused responses with a resolution of 2 ft after using 2D SF algorithm. It can be found that response characteristics before and after using SF algorithm are consistent, and there is no improvement in the resolution of the focused signals, which is consistent with the conclusion. Then, the last track is a comparison of the refocused responses (black dotted lines) by 1D SF algorithm for the borehole corrected responses with the measured AIL data by 2D SF algorithm (red solid lines). The response characteristics and

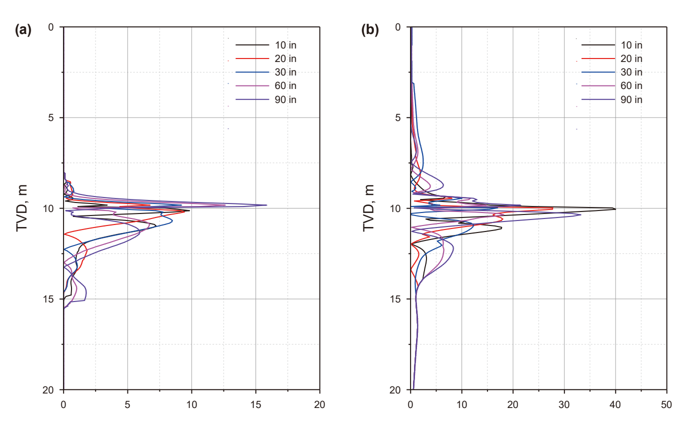

Fig. 10. Relative errors of focused responses obtained by Express and our method in different resistivity contrast formations when $\alpha = 89°$: **(a)** $C = 2$; **(b)** $C = 4$.

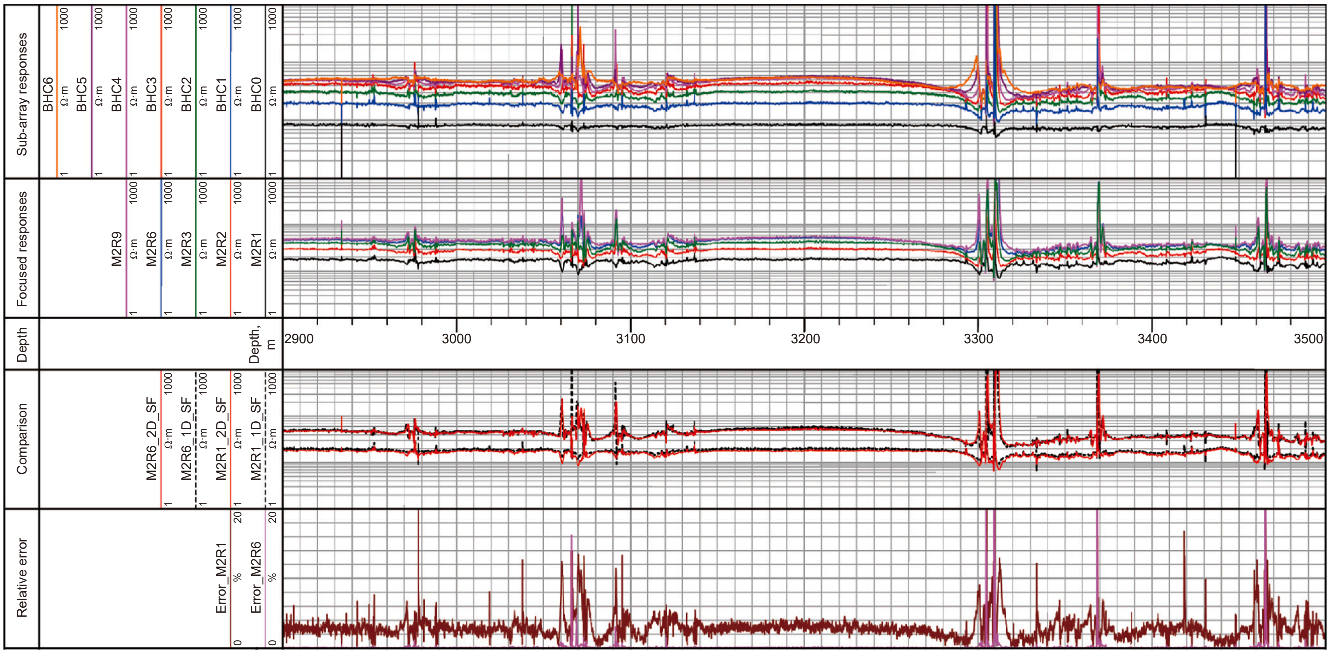

Fig. 11. Measured AIL responses of horizontal well in shale oil reservoir.

values of both are basically the same. The fourth track further gives the relative error of the focus results of the two algorithms, and the average relative error is less than 5%, which further proves the accuracy of the 1D SF algorithm.

3. Anisotropy correction of AIL data in shale formation

3.1. Sensitivity of AIL responses to anisotropy

The anisotropy is widely developed in shale reservoirs, which leads to abnormal changes in the AIL responses. Therefore, clarifying the characteristic of the focused responses in horizontal wells in anisotropic formations is an important prerequisite for the accurate data processing. For this purpose, considering the influences of the dipping angle and anisotropy, the homogeneous anisotropic model is adopted to analyze the response before and after focusing in this part. Fig. 12(a) presents the sub-array responses with the variation of dipping angle α and the anisotropy coefficient λ in the homogeneous media when the horizontal resistivity R_h is 4 Ω·m, where $\lambda = \sqrt{R_\mathrm{v}/R_\mathrm{h}}$, R_v is the vertical resistivity.

It can be seen from the figure that the sub-array responses increase as the dipping angle rises, but the responses are always smaller than the vertical resistivity. Meanwhile, the sub-array responses increase as the anisotropy coefficient increases under the same dipping angle, and the separation between the sub-array responses becomes larger, strengthening the sensitivity to anisotropy. It should be noted that when the responses at a single dipping angle has limited sensitivity to anisotropy. Therefore, it is necessary to combine the measured responses at multiple angles (such as adjacent wells and the inclined wells, etc.) to accurately characterize the anisotropy.

Generally, the separation of sub-array responses depends not only on the anisotropy coefficient and the dipping angle but also on the horizontal resistivity. Therefore, Fig. 12(b) presents the sub-array responses under different horizontal resistivity when the anisotropy coefficient is 2. Under different dipping angles, the separation of sub-array responses is inversely proportional to horizontal resistivity. When the horizontal resistivity is greater than 4 Ω·m, the responses hardly separate. Since the resistivity of shale oil reservoirs is generally greater than 10 Ω·m, it can be considered that the

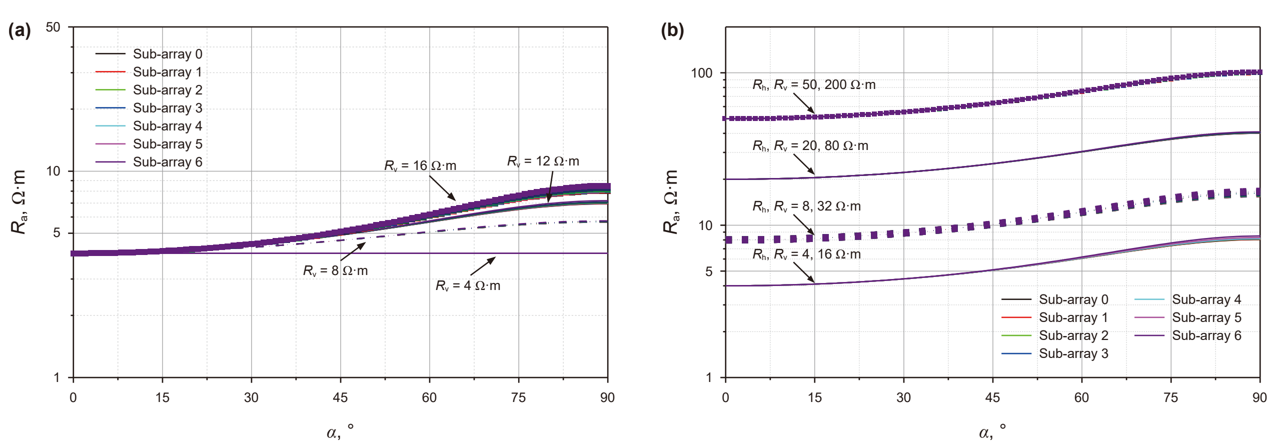

Fig. 12. Sub-array responses under different homogeneous anisotropic formations: **(a)** different anisotropy coefficients; **(b)** different horizontal resistivity.

anisotropy mainly leads to an overall increase for the sub-array responses in horizontal wells of shale oil reservoirs.

On this basis, to clarify the impact of the anisotropy on SF algorithm, Fig. 13 presents the focused responses after focusing on the sub-array responses shown in Fig. 12. It can be found that the characteristics of sub-array responses and focused responses remain consistent under different anisotropic formations, and anisotropy will not affect the applicability of SF algorithm.

3.2. Decomposition of thickness and anisotropy effects

Apart from the influence of dipping angle, the coupling of thickness and anisotropy in horizontal wells has led to the situation where the existing processing methods can only adopt the 1D inversion model. Due to the large number of inversion parameters of this model and its heavy reliance on the speed of 1D forward modeling, which makes it difficult to process in real time. However, according to the conclusions in Sections 2.3 and 3.1, the change of thickness mainly affects the separation of focused responses, and the anisotropy mainly causes an overall increase for the focused responses. Theoretically, the influences of the two are not coupled with each other.

To verify the accuracy of the above analysis, the Fig. 14(a) show the focused responses of a three-layer model when $\alpha = 89°$. In this model, each layer is an isotropic medium, the surrounding rocks resistivities are 5 Ω·m, and the middle layer resistivity is 20 Ω·m. Then, each layer is changed to an anisotropic medium with an anisotropy coefficient $\lambda = 2$, and Fig. 14(b) presents the focused responses of the modified anisotropic model. It can be found that except for the values of the responses, the response characteristics of the two models are consistent, and anisotropy only leads to an overall increase for the focused response.

To further verify this conclusion, we divide a fixed coefficient for focusing response of each detection mode in the anisotropic model, and the results are shown by the dotted lines in Fig. 14(c). The solid lines in Fig. 14(c) are the focused responses of isotropic model. The focused response after dividing the coefficients overlaps with the responses of the isotropic model. The above phenomena demonstrate that the influences of anisotropy and thickness are not coupled with each other in layered formation. Therefore, the 1D inversion model is simplified to the zero-dimension (0D) inversion model. For the influence of thickness, the thickness correction can be realized by constructing the thickness correction coefficient library.

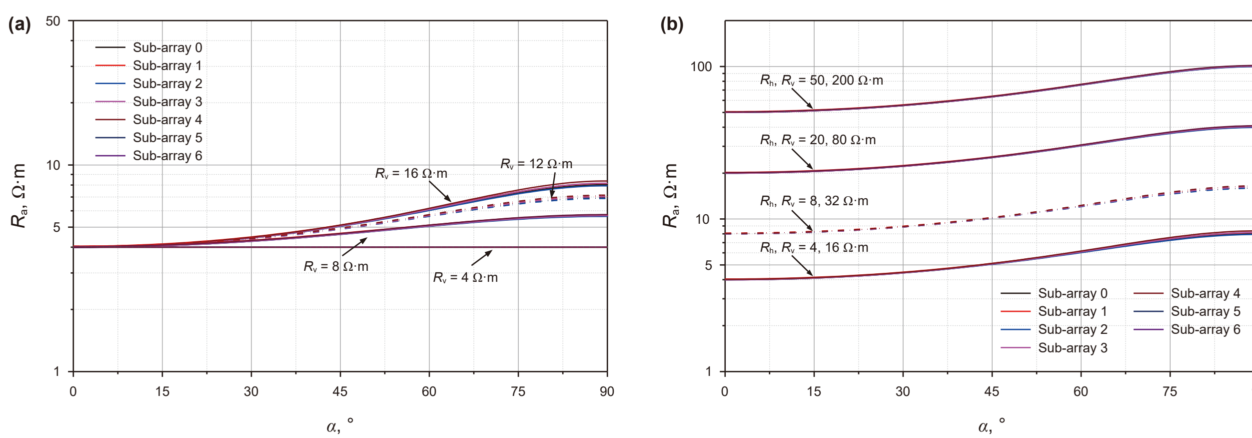

Fig. 13. Focused responses under different homogeneous anisotropic formations: **(a)** different anisotropy coefficients; **(b)** different horizontal resistivity.

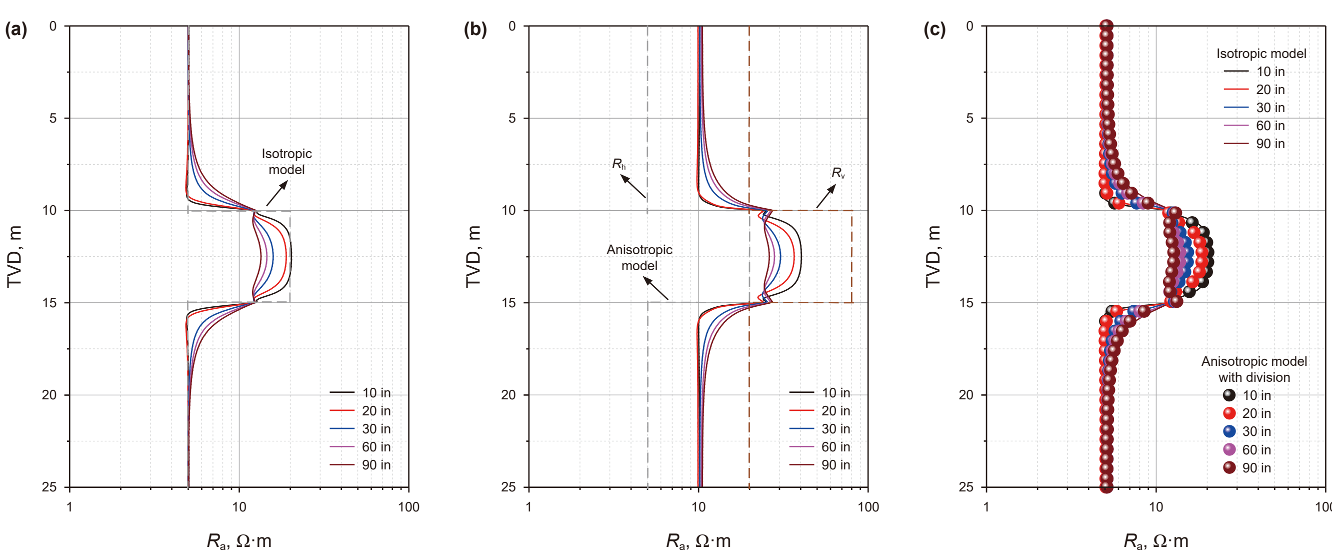

Fig. 14. Comparison of responses in an isotropic model with responses in an anisotropic model when $\alpha = 89°$: **(a)** responses of isotropic model; **(b)** responses of anisotropic model; **(c)** comparison of responses between isotropic model and anisotropic model with division.

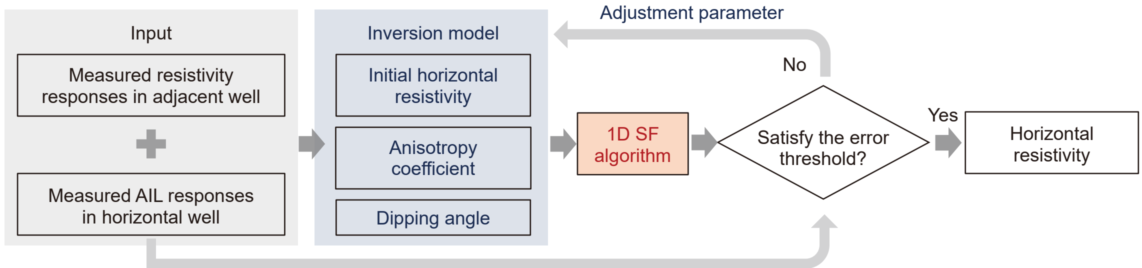

Fig. 15. Anisotropy correction process of AIL data in horizontal well.

3.3. Efficient anisotropy correction method in horizontal wells

Based on the above conclusions, this part establishes an efficient anisotropy correction method for AIL data by using Levenberg-Marquardt (L-M) algorithm (Levenberg, 1944) based on the 1D SF algorithm of radial focused responses. This method operates by taking in the dipping angle, the measured focused responses, and the anisotropy coefficient of the current measurement point. Through iterative inversion procedures, it achieves the precise extraction of horizontal resistivity. The specific inversion process is illustrated in Fig. 15.

During the above process, the anisotropy coefficient λ can be obtained from the measured resistivity responses of the adjacent well corresponding to the horizontal well, and its estimation formula can be written as follows:

$$\lambda = \frac{\sin\alpha}{\sqrt{\frac{R_h^2}{R_a^2} - \cos^2\alpha}} \tag{9}$$

where α represents the dipping angle of the measurement point. R_h is the measured resistivity of the adjacent well, and it usually adopts the average value of the deep laterolog response. Generally, the anisotropy coefficient λ of the horizontal well is a constant value, so apparent resistivity R_a can adopt the average value of the measured AIL responses in the horizontal well. Additionally, considering that the response of 10 inches may be severely affected by the borehole, it is recommended to obtain R_a based on the response of 20 inches or 30 inches.

To preliminarily validate the accuracy of the new method, Fig. 16 presents the measured resistivity data of horizontal well in a shale oil reservoir. Drillcore sampling results reveal that the anisotropy coefficient of this reservoir is roughly 1.8. In this figure, the first track depicts the phase difference (PD) and amplitude ratio (AR) responses measured by the LWD resistivity tool in this horizontal well. The LWD tool has a source spacing of 36 inches, a coil spacing of 8 inches, and two frequencies of 400 kHz and 2 MHz. The second track shows the measured AIL responses of HDIL tool. Leveraging the L-M method for PD and AR responses of two frequencies can inverse the horizontal resistivity of this reservoir, as denoted by the black solid line in the second track of the figure.

Upon comparing the measured AIL responses with the horizontal resistivity, it becomes evident that the overall values of the former are higher than those of the latter. After applying the

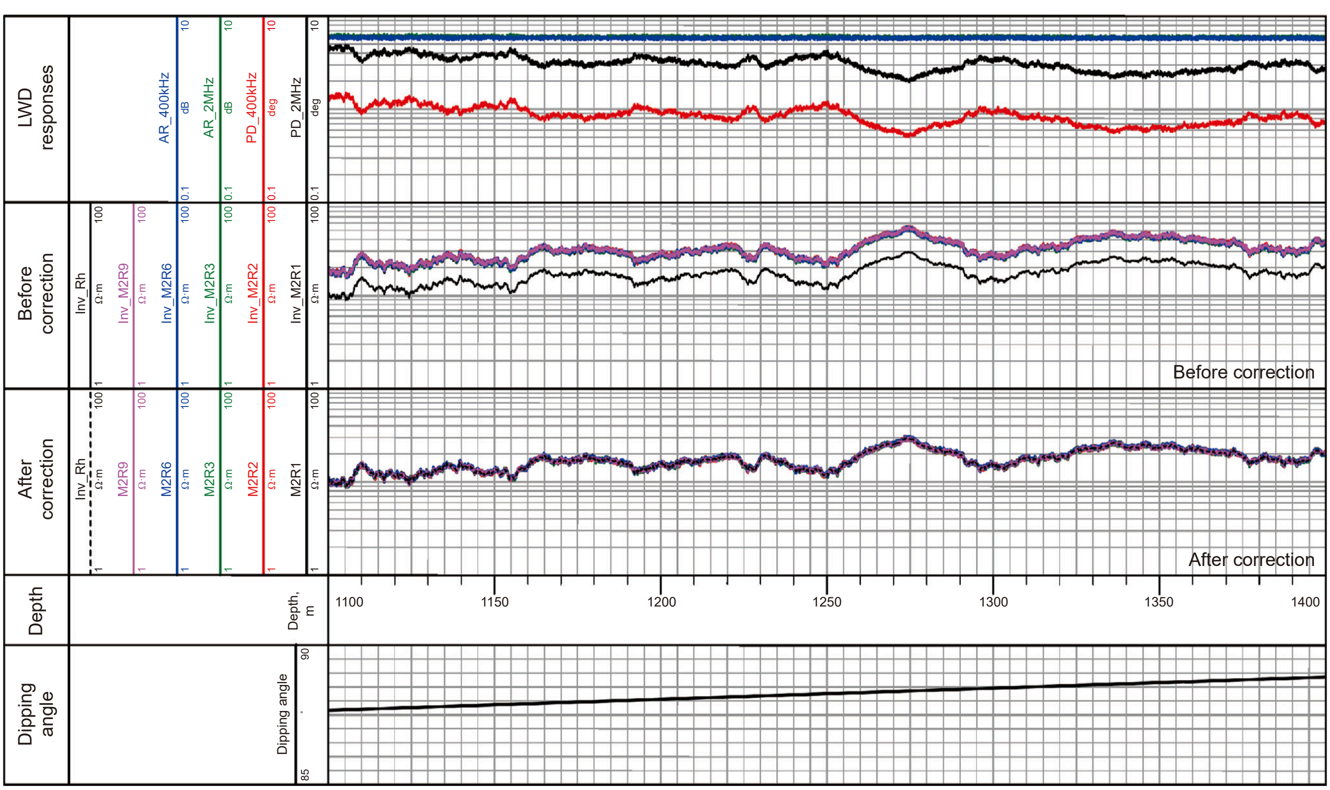

Fig. 16. Verification of anisotropy correction method for AIL responses in horizontal well.

anisotropy correction method elaborated in this section to invert the AIL responses, the corrected AIL responses are presented in the third track, and the black dashed line in the third track is the horizontal resistivity. Notably, the corrected AIL responses essentially match the values of the horizontal resistivity, thereby providing preliminary verification for the accuracy of the new method.

In the inversion process, the accuracy of the inversion depends mainly on the determination of the anisotropy coefficients. However, in the case of thin reservoirs (<5 m), the AIL response is significantly affected by reservoir thickness. As a result, it does not accurately reflect the resistivity values, leading to inaccuracies in the anisotropy coefficients calculated using Eq. (9). Consequently, the new method must incorporate thickness corrections when processing AIL data for thin beds. Furthermore, this method is specifically designed for horizontal Wells, especially when the dipping angle exceeds 80°, and the effect is good. In vertical or inclined wells (dipping angle <70°), vertical effects cannot be easily neglected, rendering the 1D SF algorithm inapplicable. Under such circumstances, the traditional 2D SF algorithm remains the preferred choice for accurate data interpretation.

4. Applications in field cases

4.1. Application in Well-I

To verify the effect of the anisotropy correction method in this paper, horizontal Well-I in the shale oil reservoir shown in Fig. 17 was selected as the test well. This well was measured using the HRAI tool of Halliburton company, and the dipping angle of the horizontal well ranged from 75° to 81°. Drillcore sampling results showed that the anisotropy coefficient of this reservoir was 1.3. In this figure, the fifth track shows the measured focused responses, and the fourth track shows the responses corrected by the anisotropy correction method presented in this paper. The third track shows the horizontal resistivity and the vertical resistivity after inversion.

In Fig. 17, the first track compares the correction results of the measured data by the commercial software LogXD™ (Maxwell Dynamics, 2017) (blue solid line) and our method (black solid line), respectively. It can be found that the responses after anisotropy correction decline significantly, effectively eliminating the responses elevation caused by anisotropy, and the correction results of the two methods basically overlap. The second track shows the relative error between the two methods, and the average error can be controlled within 3%, verifying the accuracy of the new method. Additionally, the inversion speed of the new method is about 300 points per second, which can be increased by more than 50 times compared with the LogXD™, meeting the real-time processing requirements.

For the anisotropy correction in LogXD™, we used the default parameter settings recommended by the software vendor for shale reservoir data processing, as these settings are designed to be applicable for general cases. In our method, the parameters such as the initial guess of horizontal resistivity for the Levenberg-Marquardt inversion are based on the average resistivity values from adjacent wells or regional geological data. The anisotropy coefficient is calculated as described in the manuscript, using the formula $\lambda = \sqrt{R_v/R_h}$, and estimated from the measured resistivity responses of the adjacent well and horizontal well. The version of LogXD^{TM} used in the comparison is LogXD™ released by Maxwell Dynamics Inc. The method in this paper adopts Visual Fortran 2013 as the development platform and independently develops the software to implement the new method. The parameters of computing platform used in this section are Windows 10 64-bit Professional 21H2 OS, an Intel(R) Core (TM) i9-9900 CPU, and 16 GB memory.

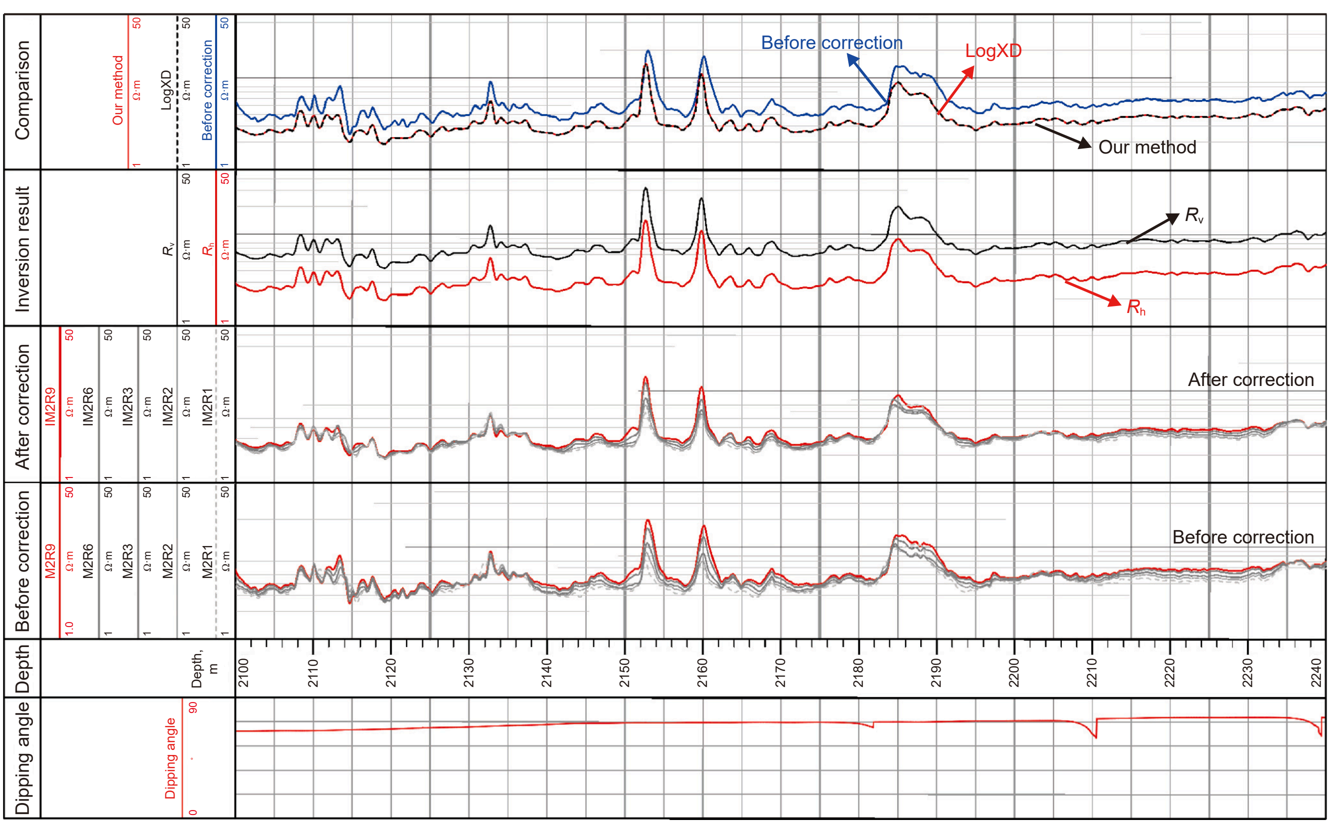

Fig. 17. Anisotropy correction of AIL data in Well-I of the shale oil reservoir.

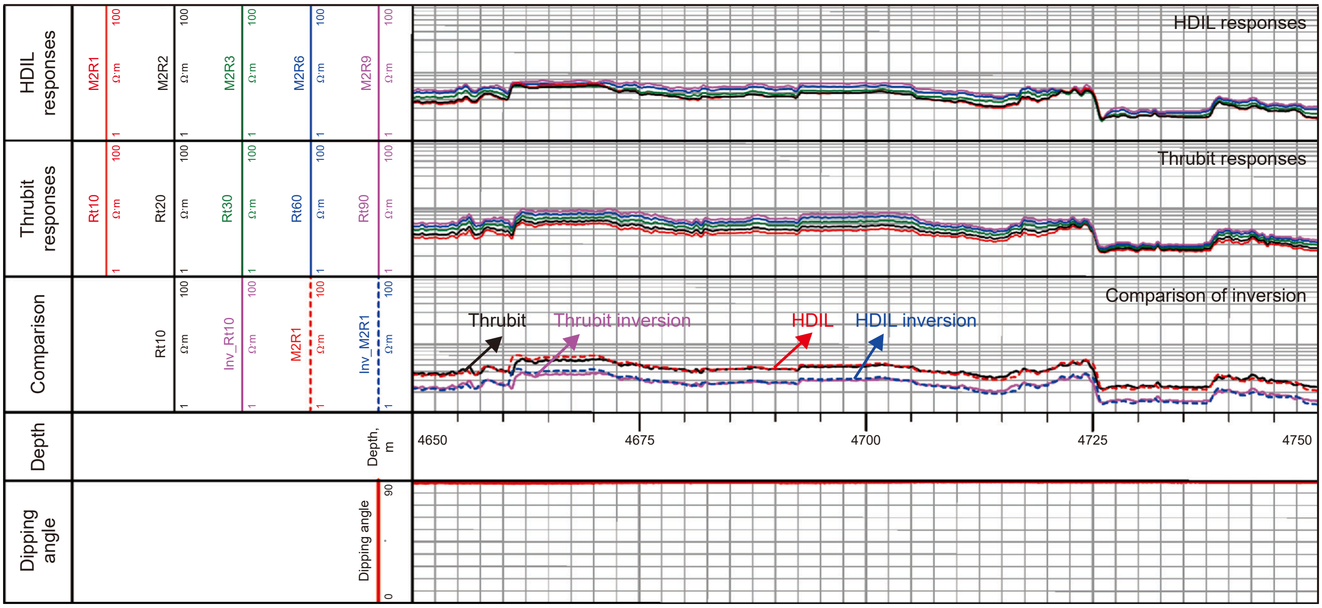

Fig. 18. Anisotropy correction of responses for different AIL tools in Well-II of shale reservoir.

4.2. Application in Well-II

To verify the applicability of the new method, Fig. 18 shows the measured AIL responses of two different tools in Well-II of the shale oil reservoirs. The dipping angle α of this well is approximately 89°, and the average of the deep laterolog response in the adjacent well is approximately 5 Ω·m. In the figure, the first track and the third track show the measured responses of the HDIL tool from Baker-Atlas and the Thrubit AIL tool (Schlumberger, 2020) from Schlumberger in the Well-II, respectively. The Thrubit AIL tool has one transmitter and eight groups of receiver pairs. The spacings of eight main receivers are 6, 9, 12, 15, 21, 27, 39 and 72 inches, respectively. It provides five median depths of investigation. The incorporated mud resistivity sensor provides critical data for making corrections and analyzing borehole fluids.

As can be seen in Fig. 18, the measured responses of the HDIL and Thrubit tools are basically the same. This shows that in the same environment, although the tools are from different companies, the trend and resolution of the measured resistivity of the formation are similar, which indicates that the two tools have the same basic ability to detect the formation, and also verifies once again that the vertical focusing in the HDIL tool is invalid in horizontal well. The Thrubit tool has a more pronounced response separation. This separation is usually related to the formation properties as well as the accuracy and sensitivity of the tools. In this figure, the more pronounced separation may indicate that it is more sensitive to variations in resistivity, and is able to more finely resolve differences in resistivity at different depths. This may be due to its unique design, which allows it to acquire richer information during the measurement.

Based on the responses of the two AIL tools, the average apparent resistivity R_a of the Well-II is approximately 8 Ω·m. By substituting the apparent resistivity R_a, dipping angle, and the average resistivity of the adjacent well into Eq. (5), the anisotropy coefficient can be estimated to be approximately 1.6. The measured responses from the two AIL tools were processed using the method proposed in this paper. The fifth track in Fig. 18 shows a comparison of the correction results of the 10 inches responses for the two tools. Here, the black solid lines represent the 10 inches responses of the two tools, and the red dashed lines represent the 10 inches responses after anisotropy correction.

It can be observed that the correction results of the two tools are basically consistent, verifying that the new method can be applied to tools from different company tools. Meanwhile, the responses after anisotropy correction are concise with the resistivity of the adjacent well, solving the elevation of the measured responses caused by anisotropy and improving the accuracy of resistivity extraction in shale oil reservoirs.

5. Conclusions

This paper comprehensively analyzed the characteristics of sub-array responses and focused responses in horizontal wells. Compared with the focused responses, the sub-array responses have stronger ability of detection boundary and richer formation information, and are less likely to generate nonlinearity and "horns" that exceed the true resistivity. Generally, the sub-array responses are more suitable for AIL data processing in horizontal wells. It is recommended to retain the sub-array responses to facilitate further data processing and interpretation.

The applicable scope of SF algorithm in horizontal wells was clarified and the focused responses for inversion were optimized. The SF algorithm is more applicable to formations with the resistivity contrast less than 4 and the thickness greater than 5 m. Within this range, the responses of 20 inches and 30 inches can reflect the true resistivity more accurately, and it is recommended to use these two responses for inversion. Additionally, the non-necessity of vertical focusing in horizontal wells was well proved. On this basis, a 1D SF method for radial focused responses was constructed, which skillfully avoided the secrecy of the 2D SF algorithm and could realize the rapid simulation of radial focused responses.

The sensitivity of AIL responses to anisotropy was analyzed. Anisotropy does not affect the applicable scope of SF algorithm. Its existence mainly causes the overall elevation of responses and hardly leads to separation. Meanwhile, the measured responses at a single dipping angle cannot accurately characterize anisotropy, and the anisotropy correction requires the combination of multiangle measured responses. Besides, the effects of anisotropy and thickness are not coupled and can be corrected in stages. Verification of field cases, compared with the commercial software LogXD™, the correction error of the new method is less than 3%, and the speed can be increased by more than 50 times, which is approximately 300 points per second. Meanwhile, the new method is applicable to the AIL tools of multiple companies.

CRediT authorship contribution statement

Lei Wang: Writing – review & editing, Supervision, Funding acquisition. **Kang-Kang Wu:** Writing – review & editing, Validation, Investigation. **Ying-Ming Liu:** Supervision, Funding acquisition, Conceptualization. **Xiao-Kai Xu:** Resources, Data curation. **Shao-Gui Deng:** Conceptualization, Supervision. **Ping Qiao:** Validation, Investigation, Writing – original draft.

Declaration of competing interest

The authors declare that they have no known competing financial interests or personal relationships that could have appeared to influence the work reported in this paper.

Acknowledgements

This work was supported in part by the Oil & Gas Major Project of China, Grant No. 2025ZD1401105; National Natural Science Foundation of China, Grant Nos. 42474152, U23B2086 and 42374150; Shandong Provincial Natural Science Foundation, Grant No. ZR2023MD053; the CNPC Innovation Foundation, Grant No. 2024DQ02-0152.

References

Alpak, F.O., Dussan, V., Habashy, T.M., et al., 2003. Numerical simulation of mud filtrate invasion in horizontal wells and sensitivity analysis of array induction tools. Petrophysics 44 (6), 396–411.

Alpak, F.O., Torres-Verdín, C., Habashy, T.M., 2006. Petrophysical inversion of borehole array-induction logs: Part I–Numerical examples. Geophysics 71 (4), 101–119. https://doi.org/10.1190/1.2213358.

Anderson, B.I., Barber, T.D., Luling, M.G., 1995. The response of induction tools to dipping, anisotropic formations. In: SPWLA 36th Annual Logging Symposium. Paris, France.

Bai, Y., Yang, S.W., Ma, Y.G., et al., 2018. Adaptive borehole correction of three-dimensional array induction logging data in a vertical borehole. Chin. J. Geophys. 61 (9), 3876–3888. https://doi.org/10.6038/cjg2018L0082 (in Chinese).

Bang, J., Solstad, A., Mjaaland, S., 2001. Formation electrical anisotropy derived from induction-log measurements in a horizontal well. SPE Reservoir Eval. Eng. 4 (6), 483–488. https://doi.org/10.2118/75115-PA.

Barber, T.D., Rosthal, R.A., 1991. Using a multiarray induction tool to achieve high-resolution logs with minimum environmental effects. In: SPE Annual Technical Conference and Exhibition, Dallas, Texas. https://doi.org/10.2118/22725-MS.

Barber, T.D., Orban, A., Hazen, G., et al., 1995. A multiarray induction tool optimized for efficient well site operation. In: SPE Annual Technical Conference and Exhibition, Dallas, Texas. https://doi.org/10.2118/30583-MS.

Beard, D.L., Zhou, Q., Bigelow, E.L., 1996. A new, fully digital, full-spectrum induction device for determining accurate resistivity with enhanced diagnostics and data integrity verification. In: SPWLA 37th Annual Logging Symposium, New Orleans, Louisiana..

Beste, R., Hagiwara, T., King, G., et al., 2000. A new high resolution array induction tool. In: SPWLA 41th Annual Logging Symposium,. Dallas, Texas.

Gao, J., Zhao, A.B., Peng, F., et al., 2007. Inversion of array induction logs and its application. Pet. Sci. 4 (3), 31–35. https://doi.org/10.1007/s12182-007-0005-x.

Ge, X.M., Ishag, M., Li, H.Y., et al., 2025. A hybrid inversion algorithm to obtain the resistivity of the uninvaded zone based on the array induction log. Comput. Geosci. 194, 105766. https://doi.org/10.1016/j.cageo.2024.105766.

Gorbatenko, A.A., Sukhorukova, K.V., 2016. High-frequency induction logging in deviated and horizontal wells: Geosteering and inversion. Russ. Geol. Geophys. 57 (7), 1111–1117. https://doi.org/10.1016/j.rgg.2016.06.010.

Hagiwara, T., 2011. Apparent dip and apparent anisotropy from multifrequency triaxial induction measurements. Geophysics 76 (1), F1–F13. https://doi.org/10.1190/1.3511349.

He, Z.B., Wu, D., Fan, Y., 2012. Skin effect correction method of multi-frequency array induction. In: International Conference on Energy, Natural Resources and Sustainable Development, pp. 361–363.

Hong, D.C., Li, N., Han, W., et al., 2021. An analytic algorithm for dipole electromagnetic field in fully anisotropic planar-stratified media. IEEE Trans. Geosci. Rem. Sens. 59 (11), 9120–9131. https://doi.org/10.1109/TGRS.2020.3040193.

Hou, J.S., Bittar, M., 2010. Correction for the borehole effect of multi-component array induction log data. In: Process in Electromagnetics Research Symposium Proceedings,. Cambridge, USA.

Hu, S.Y., Huang, W.H., Yao, H.S., et al., 2020. A correction method based on geometric factor for resistivity log response of thinly laminated sand reservoirs: A case study. Interpretation J. Sub. 9 (1), T275–T281. https://doi.org/10.1190/INT-2020-0080.1.

Kong, J.A., 1972. Electromagnetic fields due to dipole antennas over stratified anisotropic media. Geophysics 37 (6), 985–996. https://doi.org/10.1190/1.1440321.

Levenberg, K., 1944. A method for the solution of certain non-linear problems in least squares. Q. Appl. Math. 2 (2), 164–168. https://doi.org/10.1090/qam/10666.

Li, H., Yuan, C., Li, C.L., et al., 2019. Pseudo-focusing processing of array induction logging measurements in high-angle wells. In: SPWLA 60th Annual Logging Symposium, Texas, USA. https://doi.org/10.30632/T60ALS-2019_IIIII.

Liu, Z.Y., Zhang, B.Q., Zhang, C.G., et al., 2020. Response characteristics of an array induction tool (HDIL) in heterogeneous anisotropic formations. Petrophysics 61 (1), 72–85. https://doi.org/10.30632/PJV61N1-2020a2.

Løseth, L., Ursin, B., 2007. Electromagnetic fields in planarly layered anisotropic media. Geophys. J. Int. 170, 44–80. https://doi.org/10.1111/j.1365-246X.2007.03390.x.

Mallan, R.K., Torres-Verdín, C., 2007. Effects of geometrical, environmental, and petrophysical parameters on multi-component induction measurements acquired in high-angle wells. Petrophysics 48 (4), 271–288.

Mohaghegh, S.D., 2013. Reservoir modeling of shale formations. J. Nat. Gas Sci. Eng. 12, 22–33. https://doi.org/10.1016/j.jngse.2013.01.003.

Maxwell Dynamics, 2017. Products – LogXD™. https://www.maxwelldynamics.com.

Rabinovich, M., Tabarovsky, L., Corley, B., et al., 2006. Processing multi-component induction data for formation dips and anisotropy. Petrophysics 47 (6), 506–526.

Schlumberger, 2020. Through-the-bit Logging Services Slim Multiconveyance Formation Evaluation Tools. https://www.slb.com.

Tarouilly, L., Rabinovich, M., Wang, T., et al., 2003. 3D Simulation of array induction logging in a deviated well environment: A Mahakam Delta case study. In: SPE Annual Technical Conference and Exhibition, Denver, Colorado. https://doi.org/10.2118/84600-MS.

Wang, H.N., 2011. Adaptive regularization iterative inversion of array multicomponent induction well logging datum in a horizontally stratified inhomogeneous TI formation. IEEE Trans. Geosci. Rem. Sens. 49 (11), 4483–4492. https://doi.org/10.1109/TGRS.2011.2142187.

Wang, L., Deng, S.G., Xie, G.B., et al., 2022. A new deep-reading look-ahead method in electromagnetic logging-while-drilling using the scattered electric field from magnetic dipole antennas. Pet. Sci. 19 (1), 180–188. https://doi.org/10.1016/j.petsci.2021.09.035.

Wang, L., Qiao, P., Li, Z.Q., et al., 2023. A new semianalytical algorithm for rapid simulation of triaxial electromagnetic logging responses in multilayered biaxial anisotropic formations. Geophysics 88 (2), D115–D129. https://doi.org/10.1190/geo2021-0714.1.

Wei, K.J., Qin, Z., Wang, C., et al., 2024. Response characteristics and novel understandings of dual induction logging of horizontal wells in fractured reservoirs. J. Appl. Geophys. 225. https://doi.org/10.1016/j.jappgeo.2024.105393.

Zhao, J., Pei, H.C., Luo, L., et al., 2025. Anisotropic response characteristics of array induction logging in laminated shale and its correction methods. SPE J. 30 (2), 729–742. https://doi.org/10.2118/223961-PA.

Zhou, F., Meng, Q.X., Hu, X.Y., et al., 2016. Evaluation of reservoir permeability using array induction logging. Chin. J. Geophys. 59 (11), 4360–4371. https://doi.org/10.6038/cjg20161135 (in Chinese).

Zhou, J., Li, H., Rabinovich, M., et al., 2016. Interpretation of azimuthal propagation resistivity measurements: modeling, inversion, application and discussion. In: SPWLA 57th Annual Logging Symposium. Reykjavik, Iceland.

Zhou, Q., Beard, D., Hilliker, D.J., 1994. Induction tool resolution. SEG Technical Program Expanded Abstracts 1994, pp. 761–764. https://doi.org/10.1190/1.1931985.